

A new multivariable control concept for the falling film evaporator process

Julian Hofmann^{a,*}, Anton Ponomarev^b, Veit Hagenmeyer^a, Lutz Gröll^a

^a Karlsruhe Institute of Technology, Institute for Automation and Applied Informatics, Hermann-von-Helmholtz-Platz 1, Eggenstein-Leopoldshafen 76344, Germany

^b Saint Petersburg State University, Department of Mechanics of Controlled Motion, Universitetskaya nab. 7/9, St. Petersburg 199034, Russia

A B S T R A C T

The paper presents a new multivariable control concept for falling film evaporators (FFE). Our concept solves the major challenges encountered in modern FFE control: large transport delays, additional control of the output mass flow, coupling of controlled variables, and disturbances due to time-varying input dry matter content. The challenges are addressed together, for the first time, by the following control design. Based on a dynamic nonlinear input–output model, we consider a linearizing output transformation to enable application of classical linear control methods composed of feedforward design, disturbance rejection, and a decoupling network. Due to these features, we are able to design robust PID and PI controllers that substantially compensate plant-model mismatches. Connecting our concept to a digital twin of the plant yields good performance, which encourages future application of the design in the real-world process.

Keywords:

Falling film evaporator
Multivariable model-based control
Time delay
Digital twin

1. Introduction to the falling film evaporator process

Falling film evaporators (FFE) have a wide range of application in various industries. Especially, FFEs are very common in the food industry as part of a production line with downstream spray dryer to produce, e.g., milk or coffee powder. In this context, the FFE's main task consists in increasing the dry matter content of the liquid. Due to hygienic constraints and to ensure high product quality, FFEs are often built up of multiple passes enabling slow and cautious evaporation of the liquid at low temperatures under partial vacuum.

More precisely, we consider an FFE with four passes shown in Fig. 1, which represents the application discussed in this paper. At the input, liquid with mass flow \dot{m}_i and dry matter content w_i enters Plate 1, where it is distributed over the Tubes of the first pass. Inside the Tubes, the liquid flows down as thin film and partially evaporates as the outside of the Tubes is heated by the vapor contained in the Heat Chamber. The process is initialized by introducing the live steam mass flow $\dot{m}_{v,init}$ into the Heat Chamber. During stationary operation, evaporation of the liquid is caused by the process-generated vapor. To this end, the Compressor conveys the process-generated vapor from the suction side, also called Effect, to the pressure side, i.e., into the Heat Chamber. As the additional power P_C is supplied to the Compressor and thus

to the FFE process, the vapor mass flow $\dot{m}_{v,con}$ leaves the Heat Chamber. Thereby, the energy in Effect and Heat Chamber is kept in balance and split-range control of the Effect temperature ϑ_E via $\dot{m}_{v,init}$ and $\dot{m}_{v,con}$ is enabled [1]. By leaving the Tubes of the first pass, the liquid falls into Reservoir 1, is pumped via Pipe 1 onto the FFE's top and enters Plate 2, from where the same procedure as described for the first pass is repeated. The liquid exits the FFE with dry matter content w_o (higher than w_i) and mass flow \dot{m}_o (lower than \dot{m}_i). Although this FFE construction increases the process' energy efficiency and output product quality, there is a demanding challenge for the control engineer, namely, large time delays originating from the liquid transport through the Tubes and Pipes. Hence, w_o and \dot{m}_o , which should be controlled by P_C and \dot{m}_i , are remarkably delayed. In addition to that, w_o and \dot{m}_o are strongly coupled [3,4] leading to another control design challenge. The main disturbances to the process are the temporal variations in the input dry matter content w_i due to imperfect mixing in the feed tank and exchanges of the emptied tank for a new one.

2. State of the art on control of falling film evaporators

PI controllers are still standard in the industry [5]. However, it is commonly known that a PI controller is unable to adequately cope with dominant time delays since it typically leads to large-amplitude, long-lasting oscillations of w_o . In particular, Winchester et al. [4] conclude that pure single-loop PI control is insufficient to reject disturbances due to w_i .

* Corresponding author.

E-mail address: julian.hofmann@kit.edu (J. Hofmann).

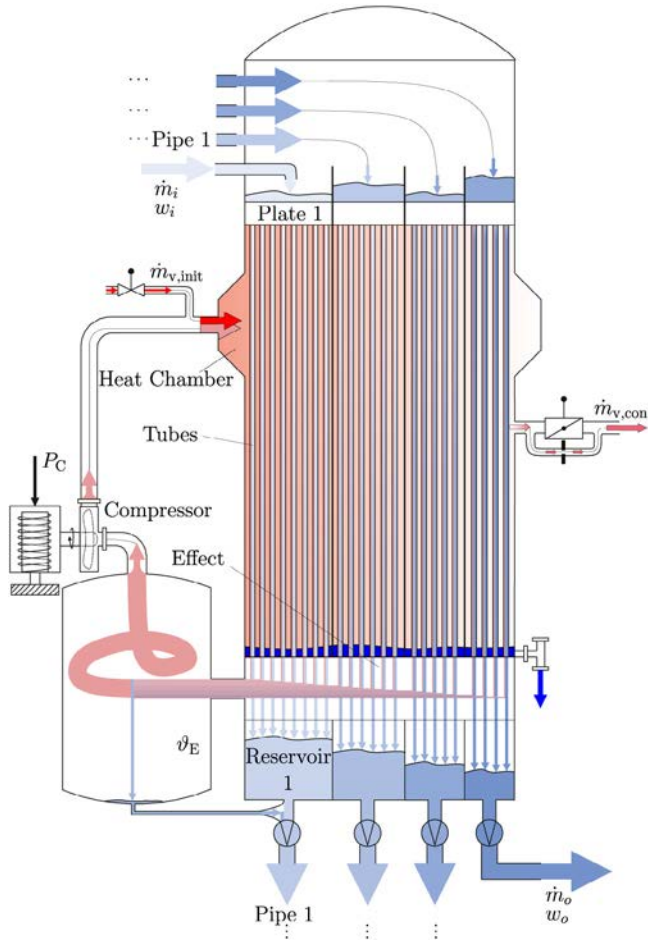


Fig. 1. Scheme of a falling film evaporator with four passes, cf. [1–3]. (For interpretation of the references to color in this figure legend, the reader is referred to the web version of this article.)

Therefore, in the last decades, more advanced methods have been proposed and applied to enhance the w_o -control loop. In [6, 7], a cascade controller based on a transfer function model is designed, where w_o is controlled via steam pressure. A similar approach based on a nonlinear process model is studied in [8] and an advanced triple loop cascade controller is developed in [9]. Moreover, Haasbroek et al. [10] design an LQR-controller with Kalman state estimator and thereby evaluate the performance of different kinds of models. Since measurements of the liquid's density, which essentially determines its dry matter content, and mass flow are usually available only at the FFE's input and output, there exist further Kalman-based approaches to estimate states between the FFE passes. In this line, Karimi et al. [11] use a linear Kalman filter to estimate the dry matter content inside the FFE (between two passes) and thus are able to design an inferential cascade controller for w_o . Another observer-based approach is treated in [12], where the observer estimates nonmeasurable disturbances, while ϑ_E and w_o are controlled by a model predictive controller (MPC). Similarly, Stefanov et al. [13] present an MPC strategy and compare it to PI control via a nonlinear partial differential equation based process model, whereas Russel [14] applies MPC to control \dot{m}_i and ϑ_E . A different approach is considered by Lahtinen [15], who develops a fuzzy controller. In [16], existing techniques, namely PI, fuzzy, cascade, and LQR control are compared w.r.t. disturbance rejection of w_i -steps, where the cascade controller revealed the best performance. Recently, Meng

et al. [17] proposed auto-tuning PID controllers to control the output dry matter content of each pass. Such an approach requires additional measurements, which are however rarely available in most FFE plants due to cost restrictions [7].

All of the aforementioned studies consider either single-loop control of w_o or multiloop control of w_o and ϑ_E . Nevertheless, besides w_o and ϑ_E , modern FFE plants should additionally enable control of \dot{m}_o . Based on the results in [3,4], this task is challenging since w_o and \dot{m}_o are strongly coupled, which requires multivariable control design. To the best of our knowledge, the only paper addressing this problem is [18], where an internal model controller (IMC) is proposed based on the models in [19]. However, the design of the IMC is not explicitly discussed therein. Furthermore, the challenge of decoupling w_o and \dot{m}_o is only solved implicitly by configuring the controller in such a way that these control loops have different response speeds.

Although modern predictor-based control techniques for uncertain time-delay systems [20–22] or systems with distributed delay [23,24] have been developed, these methods are not suitable for our application. The reasons are of practical nature. Firstly, implementation of such advanced techniques in digital control systems may be hard to do correctly, reliably, and inexpensively on the industrial level. Secondly, it is debatable if those solutions acquire acceptance among the operators. Recalling rather classical approaches such as the Smith predictor [25] and its modifications, e.g. [26,27], these approaches often lack robustness against variations of time delays [28,29]. Therefore, we make use of the robustness property of classical PI controllers excusing plant-model delay mismatches to a larger extent than the Smith predictor [30].

More precisely, we design a multivariable concept to control w_o and \dot{m}_o based on a dynamic nonlinear input–output (i/o) model. As recently shown in [3], the ϑ_E -control loop is decoupled from the control loops for w_o and \dot{m}_o , which allows to only focus on these two loops. At first, an output transformation is performed to enable control of a linear plant structure. Then, our concept can essentially be represented by a control system with two degrees of freedom (2DoF). The first DoF is the feedforward structure which ensures decoupling of control loops, disturbance rejection, and reference tracking. In this context, the method of “splitting the inverse” [31] explicitly takes time delays into account. The second DoF consists of a PID and a PI controller, which basically compensate plant-model mismatches. Therefore, an advantage of our concept is that it can be straightforwardly implemented into standard digital control systems. In a simulation study, we conclude that our concept is robust w.r.t. parametric plant-model mismatches. Finally, based on a digital twin of the plant, we validate our proposed automated ramp-up strategy and show that our concept is additionally robust w.r.t. structural plant-model mismatches.

The paper is organized as follows. In Section 3, we briefly recall our control-oriented model [3]. Based on this model, we derive our new control concept in Section 4. Besides considering the parametric robustness of the concept, it is validated via a digital twin of the plant [1] in Section 5. The main results are summarized and concluded in Section 6.

3. Control-oriented model

Our control-oriented model was originally introduced in [3]. However, since this model is the basis for our control concept, we recall relevant details of the derivation in this section. Subsequently, we convert physical variables into control nomenclature, i.e., define manipulated variables u , states x , disturbances z , and outputs y . Thus, we specify the model's state space representation, which reveals linear state equations and a nonlinear output equation. Finally, we transform the linear part of the state space model into transfer functions such that the whole model can be represented in a block diagram structure.

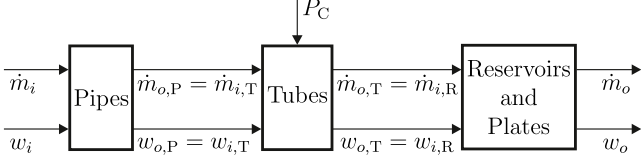


Fig. 2. Rearranged block diagram of the FFE process, cf. [3].

3.1. Derivation

Essentially, the control-oriented model originates from the full plant FFE models presented in [1,32]. The modular structure of these models offers us the opportunity to only focus on the dynamics of those modules that are relevant to determine input–output (i/o) relations for our controlled variables, namely w_o and \dot{m}_o . Another advantage is that we can aggregate the dynamics of all passes into blocks representing Pipes, Tubes, as well as Reservoirs and Plates. Since each of these blocks affects either delaying or low-pass filtering of the input variables w_i and \dot{m}_i , we can interchange these blocks without manipulating the overall i/o behavior. The rearranged block diagram is shown in Fig. 2. Note that evaporation is part of the Tubes block and induced by the power P_C supplied to the Compressor. Based on [3], we recall all relevant equations and explanations corresponding to the blocks of Fig. 2 in the following sections. The nomenclature of symbols and subscripts used in this paper is shown in Table 1.

3.1.1. Pipes

According to [1,32], the transport of liquid in Pipes is modeled as feedthrough w.r.t. mass flow, i.e.,

$$\dot{m}_{o,P}(t) = \dot{m}_i(t) \quad (1)$$

and approximated as constant delay of dry matter content such that

$$w_{o,P}(t) = w_i(t - \tau_P). \quad (2)$$

3.1.2. Tubes

The input–output dynamics of FFE Tubes [6,19,32] are given by

$$\dot{m}_{o,T}(t) = \dot{m}_{i,T}(t - \tau_T) - \frac{1}{\tau_T} \int_{t-\tau_T}^t \dot{m}_v(\theta) d\theta \quad (3)$$

for the mass flow and

$$w_{o,T}(t) = \frac{\dot{m}_{i,T}(t - \tau_T) w_{i,T}(t - \tau_T)}{\dot{m}_{o,T}(t)} \quad (4)$$

for the dry matter content. Note that multiplication of (4) by $\dot{m}_{o,T}(t)$ yields

$$\dot{m}_{o,T}(t) w_{o,T}(t) = \dot{m}_{i,T}(t - \tau_T) w_{i,T}(t - \tau_T), \quad (5)$$

which can physically be interpreted as dry matter flow balance over the Tubes. The stationary energy balance over the Compressor with efficiency factor η_C leads to the relation

$$\dot{m}_v(t) = \bar{q} P_C(t), \quad \text{where } \bar{q} = \frac{Q_{v,E} \eta_C}{p_{v,H} - p_{v,E}}. \quad (6)$$

By considering the same vapor mass flow \dot{m}_v in (3) as in (6), we assume that the vapor mass flow conveyed by the Compressor is equal to the mass flow evaporating from the liquid. This assumption is physically justified by the stationary mass balance of vapor over the Effect.

Since a slew rate limiter prevents fast changes of \dot{m}_v , the moving average filter term in (3) can be approximated by

$$\frac{1}{\tau_T} \int_{t-\tau_T}^t \dot{m}_v(\theta) d\theta \approx \dot{m}_v(t) \stackrel{(6)}{=} \bar{q} P_C(t). \quad (7)$$

To sum up, the advantage of modeling \dot{m}_v according to (6) is that we have a linear relation between the vapor mass flow \dot{m}_v and Compressor power P_C . In contrast, the relation between \dot{m}_v and the Compressor speed N_C is nonlinear [1,4]. Hence, it is more convenient to choose P_C as a manipulated variable in place of N_C .

Remark 1. In fact, the power P_C supplied to the Compressor is manipulated by the controller and therefore is not necessarily slow. However, as shown in Appendix B, P_C is converted into the Compressor's rotational speed N_C via a variable frequency drive and the rate of change of N_C is then limited by a slew rate limiter. The latter has the effect that the vapor mass flow \dot{m}_v is slowly time-varying which justifies the approximation (7).

3.1.3. Reservoirs and plates

As detailed in [3], the dynamics of Reservoirs and Plates can be aggregated via low-pass filters. Thus, low-pass filter are applied to the dry matter flow such that

$$\frac{d}{dt} (\dot{m}_o(t) w_o(t)) = \frac{1}{T_1} (\dot{m}_{i,R}(t) w_{i,R}(t) - \dot{m}_o(t) w_o(t)) \quad (8)$$

and to the mass flow such that

$$\frac{d}{dt} \dot{m}_o(t) = \frac{1}{T_2} (\dot{m}_{i,R}(t) - \dot{m}_o(t)). \quad (9)$$

Note that, in the derivation in [3], the low-pass filter with constant T_1 is applied to the dry matter content w_o instead of dry matter flow $\dot{m}_o w_o$, cf. (8). As being feasible from modeling perspective, the advantage of (8) is that the nonlinearity will appear in the output equation $w_o = (\dot{m}_o w_o) / \dot{m}_o$ instead of the state equations. Therefore, the state equations are linear, see Section 3.3.

3.1.4. Input–output model

Next, we can combine (1)–(9) to obtain compact i/o relations in terms of mass flow and dry matter flow. Plugging (2) into (5) into (8) leads to

$$\frac{d}{dt} (\dot{m}_o(t) w_o(t)) = \frac{1}{T_1} (\dot{m}_i(t - \tau_T) w_i(t - \tau_T - \tau_P) - \dot{m}_o(t) w_o(t)) \quad (10)$$

$$\approx \frac{1}{T_1} (\dot{m}_i(t - \tau_T - \tau_P) w_i(t - \tau_T - \tau_P) - \dot{m}_o(t) w_o(t)) \quad (11)$$

where the approximation (11) enables remarkable simplification of the later control design while the induced model error is comparatively small. At this point, the reader might remark that the approximation

$$\frac{d}{dt} (\dot{m}_o(t) w_o(t)) \approx \frac{1}{T_1} (\dot{m}_i(t - \tau_T) w_i(t - \tau_T) - \dot{m}_o(t) w_o(t)) \quad (12)$$

may also be feasible. However, we have observed in identification experiments that considering (11) instead of (12) models the i/o dynamics more accurately, cf. Fig. 3. Combining (1), (3), (7), and (9) yields

$$\frac{d}{dt} \dot{m}_o(t) = \frac{1}{T_2} (\dot{m}_i(t - \tau_T) - \bar{q} P_C(t) - \dot{m}_o(t)). \quad (13)$$

To sum up, the i/o dynamics are composed of (11) and (13).

Remark 2. While the Pipe delay τ_P is of the “hydraulic type” [33], the Tube delay τ_T is more complicated because the Tubes, unlike Pipes, are not fully filled with liquid which may lead to

Table 1
Symbol and subscript nomenclature.

Symbol and description	SI unit	Subscript and description
K_v	Flow factor	kg s^{-1}
$K_{v,s}$	Open valve flow factor	kg s^{-1}
\dot{m}	Mass flow	kg s^{-1}
N	Rotational speed	s^{-1}
p	Pressure	Pa
P	Power	W
s	Frequency variable	s^{-1}
t	Time	s
T	Time constant	s
v	Valve position	-
w	dry matter content	kg kg^{-1}
η	Efficiency factor	-
ϑ	Temperature	K
ϱ	Density	kg m^{-3}
τ	Time delay	s

Symbol	Description
0	Initial value
d	Desired
C	Compressor
con	Control
E	Effect
f	Filter
H	Heat Chamber
i	Input
init	Initialization
max	Maximum
o	output
P	Pipes
R	Reservoirs and Plates
T	Tubes
v	Vapor
V	Valve

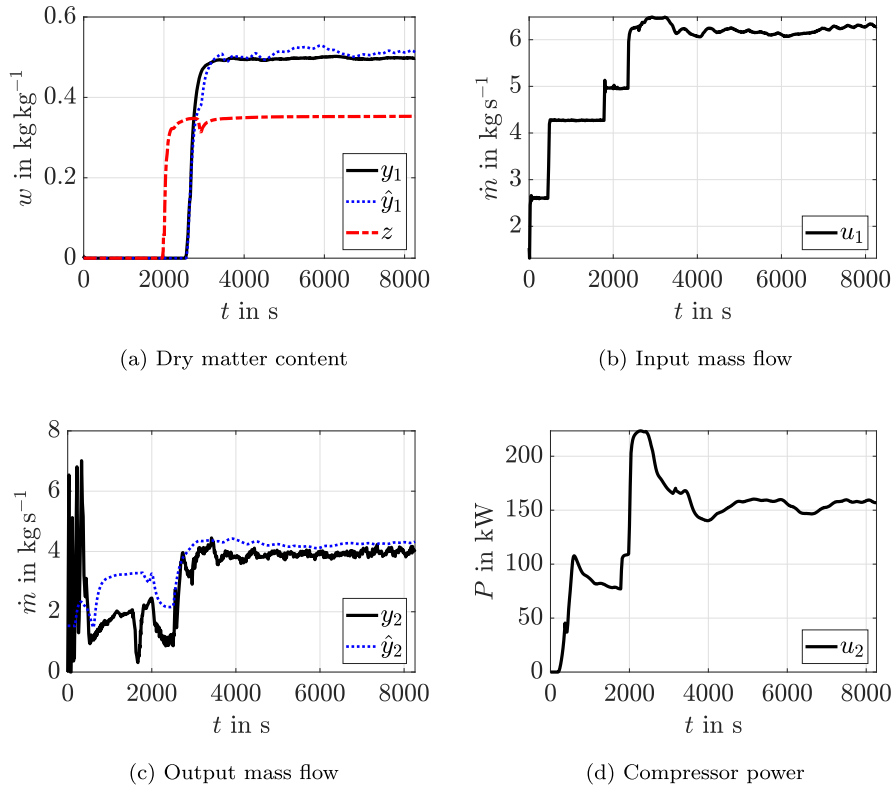


Fig. 3. Identification of the model (20) with real-world process data. Variables indicated by $\hat{(\cdot)}$ are model outputs. (For interpretation of the references to color in this figure legend, the reader is referred to the web version of this article.)

wave formation, mixing of the flow, and other effects [34,35]. As recently shown in [2,36], the Tube delay can be modeled by the concepts of Dynamic Plug Flow or Overtaking Particle Flow. The latter represents a nonlinear distributed delay model further complicated by evaporation. Additionally, there are other advanced models to describe the behavior of evaporating liquid film inside the Tubes based on coupled Navier–Stokes equations for liquid and vapor phase [37,38]. In general, both of the delays, τ_p and τ_T , depend on the liquid’s dry matter content and mass flow [1,39] which both vary due to controller action. However, in the present contribution, we assume constant τ_p and τ_T . In practical considerations, we observe that controller action causes changes of τ_T by at most $\pm 20\%$ and τ_p by at most $\pm 10\%$ w.r.t. their nominal values. Moreover, in addition to other features, we apply PID and PI controllers which are robust against delay

changes [30]. Due to these reasons, modeling constant delays is justified for our purpose.

3.2. Control nomenclature

Before converting the physical variables of the model (11), (13) into control nomenclature, we introduce the delays

$$\tau_1 := \tau_T + \tau_p, \quad (14a)$$

$$\tau_2 := \tau_T \quad (14b)$$

for the sake of compact notation. The manipulated variables are

$$\begin{bmatrix} u_1(t) \\ u_2(t) \end{bmatrix} := \begin{bmatrix} \dot{m}_i(t) \\ P_C(t) \end{bmatrix}, \quad (15)$$

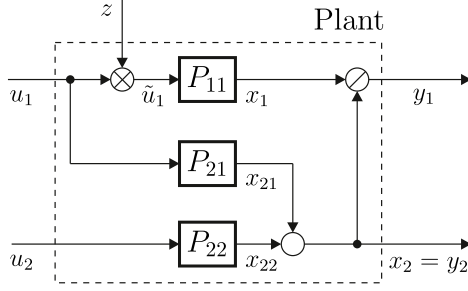


Fig. 4. Block diagram representation of the plant for control design.

the measured disturbance is

$$z(t) := w_i(t), \quad (16)$$

the state variables are

$$\begin{bmatrix} x_1(t) \\ x_2(t) \end{bmatrix} := \begin{bmatrix} \dot{m}_o(t)w_o(t) \\ \dot{m}_o(t) \end{bmatrix}, \quad (17)$$

and the outputs are

$$\begin{bmatrix} y_1(t) \\ y_2(t) \end{bmatrix} := \begin{bmatrix} w_o(t) \\ \dot{m}_o(t) \end{bmatrix}. \quad (18)$$

Remark 3. Throughout the paper, we assume that measurements of the dry matter content w or, more precisely, of $z = w_i$ and $y_1 = w_o$ are available. In fact, these variables are indirectly measured via a well-identified static estimator, which is detailed in Appendix A.

3.3. State space representation

To obtain a system of linear state equations, we additionally introduce the pseudo-input

$$\tilde{u}_1(t) := \dot{m}_i(t)w_i(t) = u_1(t)z(t). \quad (19)$$

Then, with (11), (13), and the control nomenclature in Section 3.2, we obtain

$$\begin{aligned} \begin{bmatrix} \dot{x}_1(t) \\ \dot{x}_2(t) \end{bmatrix} &= \begin{bmatrix} -\frac{1}{T_1} & 0 \\ 0 & -\frac{1}{T_2} \end{bmatrix} \begin{bmatrix} x_1(t) \\ x_2(t) \end{bmatrix} + \begin{bmatrix} 0 \\ \frac{1}{T_2} \end{bmatrix} u_1(t - \tau_2) \\ &+ \begin{bmatrix} \frac{1}{T_1} \\ 0 \end{bmatrix} \tilde{u}_1(t - \tau_1) + \begin{bmatrix} 0 \\ -\frac{\hat{q}}{T_2} \end{bmatrix} u_2(t), \end{aligned} \quad (20a)$$

$$\begin{bmatrix} y_1(t) \\ y_2(t) \end{bmatrix} = \begin{bmatrix} x_1(t) / x_2(t) \\ x_2(t) \end{bmatrix}. \quad (20b)$$

Hence, (20a) is a linear state space model with nonlinear output equation (20b).

Although being quite simple, the model (20) is well able to map the real-world process as can be seen in Fig. 3. The deviations between the measured output y_2 and model output \hat{y}_2 during $t \in [0, 2000]$ s are not of interest from control perspective since in this time span, the FFE is flooded by water, which is obvious from the plot of z in Fig. 3(a).

3.4. Block diagram representation

By applying the Laplace transformation to (20a) neglecting initial values, we find the transfer functions

$$P_{11}(s) = \frac{X_1(s)}{\tilde{U}_1(s)} = \frac{e^{-\tau_1 s}}{T_1 s + 1}, \quad (21a)$$

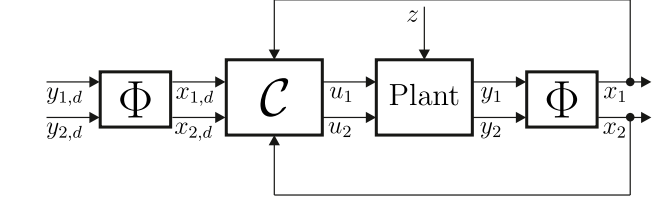


Fig. 5. Closed loop with output transformation Φ and controller c to be designed in the sequel.

$$P_{21}(s) = \frac{X_{21}(s)}{U_1(s)} = \frac{e^{-\tau_2 s}}{T_2 s + 1}, \quad (21b)$$

$$P_{22}(s) = \frac{X_{22}(s)}{U_2(s)} = -\frac{\hat{q}}{T_2 s + 1}, \quad (21c)$$

which lead to the block diagram in Fig. 4 representing (20).

4. New multivariable control concept

The design of our control concept is based on the Plant in Fig. 4 with transfer functions (21). In Section 4.1, a stepwise derivation of the concept is given. To avoid operation beyond the actuators' limits, we derive a domain of feasible setpoints in Section 4.2.

4.1. Derivation

All control features of the concept, such as feedforward or decoupling compensators, are presented in the following sections, where nonexact plant parameters indicated by $\hat{(\cdot)}$ are explicitly considered in the derivation.

4.1.1. Output transformation

Instead of directly controlling the nonlinear outputs y_1, y_2 , see (20b), we better design our controller based on the linear state space Eqs. (20a). To this end, we introduce the following output transformation:

$$\begin{bmatrix} x_1(t) \\ x_2(t) \end{bmatrix} = \begin{bmatrix} y_1(t)y_2(t) \\ y_2(t) \end{bmatrix} := \Phi(y_1(t), y_2(t)). \quad (22)$$

Hence, as shown in Fig. 5, the controller C becomes a state-based controller and will be designed in the sequel.

4.1.2. Decoupling network

In Fig. 4, we observe that y_2 is affected by u_1 via P_{21} . The latter may be interpreted as output disturbance to P_{22} . Hence, we can apply classical disturbance compensation for the purpose of decoupling such that

$$Q_{21}(s)\hat{P}_{22}(s) = \hat{P}_{21}(s), \quad (23)$$

which yields the decoupling compensator

$$Q_{21}(s) = \frac{\hat{P}_{21}(s)}{\hat{P}_{22}(s)} = -\frac{e^{-\hat{\tau}_2 s}}{\hat{q}}. \quad (24)$$

The decoupling network is shown in Fig. 6, where the feedback controllers C_1 and C_2 are designed in Section 4.1.4.

4.1.3. Feedforward design and disturbance rejection

At first, to achieve good reference tracking of $x_{1,d}$, the feedforward is designed based on P_{11} according to (21a). Since P_{11} has a delay, we cannot directly calculate its inverse as noncausal behavior would be the consequence; the latter not being realizable. Instead, we apply an idea of Kreisselmeier et al. [31] and "split

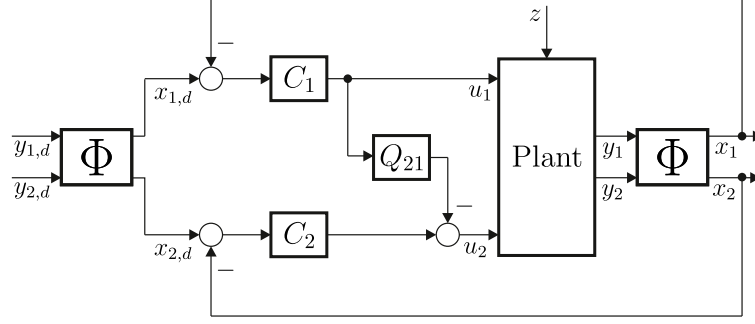


Fig. 6. Closed loop with output transformation Φ , decoupling compensator Q_{21} , and controllers C_1 and C_2 .

the inverse” into a pre-filter W_{11} and a compensator Q_{11} . To this end, let us split P_{11} such that

$$P_{11}(s) = P_{11,0}(s)e^{-\tau_1 s}, \quad (25)$$

where

$$P_{11,0}(s) = \frac{1}{T_1 s + 1} \quad (26)$$

is the delay-free part and $e^{-\tau_1 s}$ is the delayed part.

Thus, the compensator Q_{11} is determined by the inverse of $\hat{P}_{11,0}$ while the first-order low-pass filter F with time constant T_f enables properness, i.e.,

$$Q_{11}(s) = \hat{P}_{11,0}^{-1}(s)F(s) = \frac{\hat{T}_1 s + 1}{T_f s + 1}. \quad (27)$$

According to Fig. 4, the disturbance z couples into the plant via multiplication in front of P_{11} . Hence, we can easily reject this disturbance by dividing the output of Q_{11} by z .

The pre-filter W_{11} is applied to $x_{1,d}$ and composed of the delayed part $e^{-\hat{\tau}_1 s}$ of \hat{P}_{11} as well as of the filter F , cf. [31], such that

$$W_{11}(s) = e^{-\hat{\tau}_1 s} F(s) = \frac{e^{-\hat{\tau}_1 s}}{T_f s + 1}. \quad (28)$$

Thereby, we ensure that x_1 being delayed by P_{11} and $x_{1,d}$ being comparably delayed by W_{11} “meet at the right time”. Consequently, we do not control $x_{1,d}$. Instead, we control $\tilde{x}_{1,d}$, which corresponds to $x_{1,d}$ delayed and filtered by W_{11} . However, as we are interested in setpoint control, the resulting shift between $\tilde{x}_{1,d}$ and $x_{1,d}$ has no practical consequences.

To design the feedforward for P_{22} , let us consider the closed-loop system in Fig. 6. Due to the transformation Φ , changes of $y_{2,d}$ affect both control loops, the first and second one. Hence, the same filter W_{11} as applied to $x_{1,d}$ must also be applied to $x_{2,d}$. This issue needs to be considered for the design of the second loop’s compensator Q_{22} , which must then ensure that

$$X_2(s) = W_{11}(s)X_{2,d}(s) \quad (29)$$

holds, where neglecting C_2 , Q_{21} , and \hat{P}_{21} yields

$$X_2(s) = Q_{22}(s)\hat{P}_{22}(s)X_{2,d}(s). \quad (30)$$

Inserting (30) into (29) leads to

$$Q_{22}(s) = \frac{W_{11}(s)}{\hat{P}_{22}(s)} = -\frac{e^{-\hat{\tau}_1 s}}{T_f s + 1} \frac{\hat{T}_2 s + 1}{\hat{q}}. \quad (31)$$

The complete control concept is shown in Fig. 7. Note that all variables being filtered by W_{11} are marked by (\cdot) .

4.1.4. Controllers

Let us reconsider the plant in Fig. 4 and recapitulate some results from Section 4.1.1 to Section 4.1.3, namely that

- the nonlinearity (division) at the plant’s output is canceled by the output transformation Φ ,
- the influence of u_1 via P_{21} on y_2 is canceled by the decoupling compensator Q_{21} ,
- the influence of z is canceled by the division in the feedforward path after Q_{11} , see Fig. 7.

Thus, the design of C_1 and C_2 can be restricted to P_{11} and P_{22} , respectively.

From internal model control (IMC) theory [40], we know that P_{11} representing “low-pass filter plus delay” should be controlled via a PI controller with Smith predictor (PI-S). However, recalling that the Smith predictor lacks robustness to plant-model mismatches [41], we will not implement PI-S. Indeed, as shown in [2,36,39], the FFE process is well modeled as a system with distributed delays such that our approximation as a system with pointwise delays naturally leads to some model error requiring robustness of the control concept. Therefore, we instead follow the recommendation in [28], where it is argued that a PID controller outperforms PI-S w.r.t. performance-robustness trade-off. Moreover, according to [28], the derivative action of a PID controller adds a similar effect as the Smith predictor part of PI-S. Hence, we consider the PID controller

$$C_1(s) = k_{p,1} + \frac{k_{i,1}}{s} + k_{d,1}s \quad (32)$$

with gains [28]

$$k_{p,1} = \frac{2(3\hat{T}_1 + \hat{\tau}_1)}{9\hat{\tau}_1}, \quad k_{i,1} = \frac{2}{3\hat{\tau}_1}, \quad k_{d,1} = \frac{2\hat{T}_1}{9}. \quad (33)$$

Note that the PID controller gains (33) correspond to the ideal representation (32). However, for realization purposes, the D-part needs to be approximated by

$$k_{d,1}s \approx \frac{k_{d,1}\beta_1 s}{s + \beta_1}. \quad (34)$$

By applying IMC to P_{22} representing a low-pass filter, the PI controller

$$C_2(s) = k_{p,2} + \frac{k_{i,2}}{s} \quad (35)$$

with gains

$$k_{p,2} = -\frac{\hat{T}_2}{\hat{q}T_{f,2}}, \quad k_{i,2} = -\frac{1}{\hat{q}T_{f,2}} \quad (36)$$

is obtained. According to [40], a good rule of thumb is to choose the low-pass filter time constant $T_{f,2}$ two times faster than the plant’s time constant \hat{T}_2 , i.e., $T_{f,2} = \hat{T}_2/2$.

Finally, the control concept is composed of Fig. 7 with (22), (24), (27), (28), (31), (32), (34), and (35). Note that, particularly in Section 5, we explicitly distinguish between “feedforward structure” and “controllers”. Therefore, in the following, C_1 and C_2

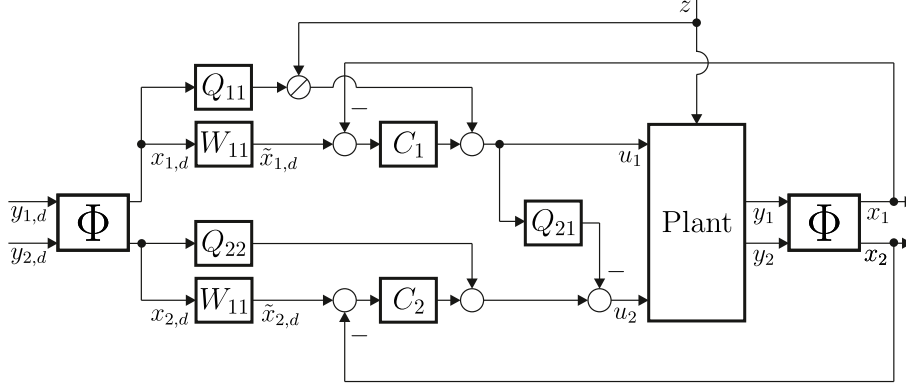


Fig. 7. Complete control concept consisting of output transformation Φ , decoupling compensator Q_{21} , feedforward compensators Q_{11} and Q_{22} , pre-filter W_{11} , disturbance rejection, as well as controllers C_1 and C_2 .

are referenced as “controllers”, while Fig. 7 without C_1 and C_2 is referenced as “feedforward structure”.

Remark 4. To sum up, our concept has the following advantages:

- Decoupling of controlled variables is *explicitly* achieved by the feedforward structure. In contrast, the *implicit* solution via different speeds of control loop responses presented in [18] is insufficient for our FFE configuration. This insufficiency is manifested in closed-loop simulations with our digital twin, where we observe large oscillations, especially of \dot{m}_o , attributed to only implicit decoupling via controller gains.
- The dominant time delays τ_p and τ_T are explicitly considered in the feedforward design by applying the method of “splitting the inverse” [31].
- Application of PID and PI controllers affects sufficient robustness w.r.t. delay changes due to controller action although the delays are modeled constant. Thus, these simple controllers are, in our case, superior to the Smith predictor and certain modifications, which lack robustness [28,30].
- Since our control concept is built from standard blocks that have well-known and tested implementations in the industrial systems, it is simpler to implement and better accepted by the operators than more modern approaches [20–22,24].

4.2. Feasible setpoint domain

Generally, the limits of the actuators should be taken into account. As FFEs usually operate with constant setpoints for long time spans, it is important to ensure that the actuators are kept away from their limits during stationary process. Therefore, a map of feasible setpoint pairs $(y_{1,d}, y_{2,d})$ is developed in this section.

At first, we consider the stationary i/o equations

$$y_{1,d} = \frac{u_{1,d} \bar{z}}{y_{2,d}}, \quad (37a)$$

$$y_{2,d} = u_{1,d} - \bar{q} u_{2,d}, \quad (37b)$$

which follow from (20) with $x_1(t) := x_{1,d} = \text{const}$, $x_2(t) := x_{2,d} = \text{const}$, $u_1(t) := u_{1,d} = \text{const}$, $u_2(t) := u_{2,d} = \text{const}$, $z(t) := \bar{z} = \text{const}$, $y_1(t) := y_{1,d} = \text{const}$, and $y_2(t) := y_{2,d} = \text{const}$. By solving (37) w.r.t. $u_{1,d}$, $u_{2,d}$, we find that

$$u_{1,d} = \frac{y_{1,d} y_{2,d}}{\bar{z}}, \quad (38a)$$

$$u_{2,d} = \frac{y_{2,d} (y_{1,d} - \bar{z})}{\bar{q} \bar{z}}. \quad (38b)$$

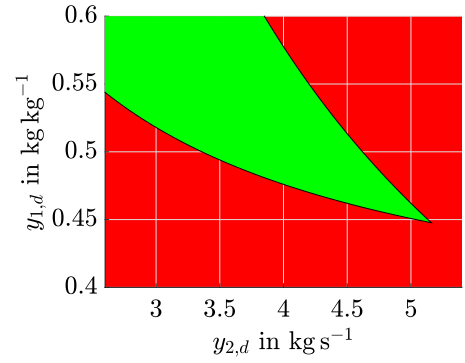


Fig. 8. Feasible (green) and infeasible (red) setpoint domains. (For interpretation of the references to color in this figure legend, the reader is referred to the web version of this article.)

The actuator limits affect that

$$u_{1,d} \in [u_{1,d,\min}, u_{1,d,\max}] = [0, 6.6] \text{ kg s}^{-1}, \quad (39a)$$

$$u_{2,d} \in [u_{2,d,\min}, u_{2,d,\max}] = [60, 200] \text{ kW}. \quad (39b)$$

In this context, note that generally, the Compressor is able to operate at lower power than 60 kW. However, in this case, there would be operation below the critical point, which is not recommended. Furthermore, the maximum value of $u_{1,d}$ corresponds to the fully opened input mass flow control valve, i.e., $v \equiv 1$ in (B.2).

Observe that (38) and (39) yield a system of inequalities, which can be solved analytically. In order to find pairs $(y_{1,d}, y_{2,d})$ such that the actuator limits (39) are met, we combine (38), (39) and find

$$y_{1,d} \leq \frac{u_{1,d,\max} \bar{z}}{y_{2,d}}, \quad (40)$$

$$y_{1,d} \leq \frac{\bar{z}(y_{2,d} + \bar{q} u_{2,d,\max})}{y_{2,d}}, \quad (41)$$

$$y_{1,d} \geq \frac{\bar{z}(y_{2,d} + \bar{q} u_{2,d,\min})}{y_{2,d}}. \quad (42)$$

Based on (40), (42), the domain of admissible pairs $(y_{1,d}, y_{2,d})$ is plotted in green for the interesting ranges of $y_{1,d}$, $y_{2,d}$ in Fig. 8, where $\bar{z} = 0.35 \text{ kg kg}^{-1}$ and $\bar{q} = 0.024 \text{ kg kW}^{-1} \text{ s}^{-1}$. Note that, in the ranges of $y_{1,d}$, $y_{2,d}$ shown in Fig. 8, the inequality (41) is inactive and can therefore be ignored. Hence, the following choice of setpoints is feasible:

- Setpoint 1: $y_{1,d} = 0.51 \text{ kg kg}^{-1}$, $y_{2,d} = 4.3 \text{ kg s}^{-1}$,
- Setpoint 2: $y_{1,d} = 0.55 \text{ kg kg}^{-1}$, $y_{2,d} = 3.8 \text{ kg s}^{-1}$.

Table 2
Simulation parameters.

Symbol	Value	Unit
T_1 ($\hat{T}_1 = 1.4 T_1$)	70.36 (98.50)	s
T_2 ($\hat{T}_2 = 0.6 T_2$)	154.1 (92.47)	s
τ_1 ($\hat{\tau}_1 = 1.4 \tau_1$)	251.0 (351.4)	s
τ_2 ($\hat{\tau}_2 = 0.6 \tau_2$)	185.0 (111.0)	s
\bar{q} ($\hat{q} = 1.4 \bar{q}$)	0.024 (0.034)	kg kW ⁻¹ s ⁻¹
T_f	100	s
$k_{p,1}$	0.41	–
$k_{i,1}$	0.003	s ⁻¹
$k_{d,1}$	15.64	s
β_1	0.028	s ⁻¹
$k_{p,2}$	–82.58	–
$k_{i,2}$	–0.54	s ⁻¹

This choice is considered for the simulations in Section 5.

5. Simulation

In this section, the control concept presented in Section 4 is tested w.r.t. parameter uncertainties, see Section 5.1, and validated via a digital plant twin in Section 5.2.

However, before the concept is simulated, we have to define a suitable test signal for the disturbance $z = w_i$. To this end, the following scenario is considered: The liquid fed into the FFE comes from a feed tank, where the dry matter content at the bottom is larger than at the top due to imperfect mixing and sedimentation. Since the outlet is at the bottom, the input dry matter content w_i is initially higher than the average \bar{w}_i and then lowers until the tank is empty. After approximately two hours, the feed tank is empty and gets replaced by a new one so that w_i increases fast. In the sequel, this behavior is simulated as a sawtooth wave for w_i , which falls from 0.36 kg kg⁻¹ to 0.34 kg kg⁻¹ within two hours and then steps back to 0.36 kg kg⁻¹.

5.1. Robustness to parameter uncertainties

The simulation model investigated in this section is composed of the plant in Fig. 4 and the control structure in Fig. 7. Additionally, consider the parameters in Table 2, where the uncertainties of the plant parameters are given in parentheses and indicated by $(\hat{\cdot})$. Note that all plant parameters are identified via output error based least squares using the digital twin being specified in Section 5.2. However, as identification is not in the scope of this paper, we will not further detail this topic.

Let us consider the following simulation scenario:

1. $t = 0$ s: Start from the stationary state.
2. $t = 2000$ s: Step from Setpoint 1 to Setpoint 2, see Section 4.2.
3. $t = 4600$ s: Step from Setpoint 2 to Setpoint 1, see Section 4.2.
4. $t = 7200$ s: Step of disturbance z due to feed tank exchange.

All simulations are performed with ideal initial conditions. Furthermore, actuator dynamics, see Appendix B, are neglected. The corresponding results are shown in Fig. 9.

Observe that, in case of no plant-model mismatches, i.e., the control structure's $(\hat{\cdot})$ -parameters exactly match the plant's parameters, y_1, y_2 overlap $\hat{y}_{1,d}, \hat{y}_{2,d}$, where the latter correspond to $y_{1,d}, y_{2,d}$ filtered by W_{11} , see (28). Furthermore, in this case, the closed-loop behavior is completely determined by the feedforward structure such that there is no contribution of the controllers C_1 and C_2 . If there are plant-model mismatches, i.e., the control structure's $(\hat{\cdot})$ -parameters are different from the plant's

parameters as shown in Table 2, the tracking and disturbance response of \hat{y}_1, \hat{y}_2 is still good although the parameter uncertainties are $\pm 40\%$. This fact emphasizes the apparent robustness of our concept. Finally, note that u_1 and \hat{u}_1 initially match exactly while there is an initial mismatch between u_2 and \hat{u}_2 . The reason for this behavior is that, \hat{u}_1 is only affected by the nonexact time constant \hat{T}_1 , see (27), which has no disturbing effects in case of ideal initial conditions. However, \hat{u}_2 is additionally affected by the nonexact parameter \hat{q} leading to a gain mismatch in the feedforward structure, see (24) and (31), and thus causes the initial mismatch of u_2 and \hat{u}_2 .

5.2. Validation via digital twin

Next, the control structure in Fig. 7 is connected to the Plant consisting of the digital twin [1]. More precisely, compared to [1], the following modifications are implemented in the digital twin of the present contribution:

1. Since the Effect model in [1] has numerical drawbacks due to its discrete-time representation, it is replaced by the Overtaking Particle Flow model with water-proportional evaporation, see [36,39]. The latter has similar behavior as the discrete-time model in [1] but has better numerical stability due to its continuous-time nature.
2. The actuator dynamics described in Appendix B are additionally included in the digital twin.

The controller parameters correspond to the ones in Table 2, where the exact parameters T_1, T_2, τ_1, τ_2 , and \bar{q} are applied since we investigate structural plant-model mismatches in this section.

Before the control structure is initialized, the FFE is flooded by water for cleaning purposes during $t \in [0, 2000]$ s. At $t = 2000$ s, the liquid to be concentrated (product) enters the FFE which is recognized by a large step of z , see Fig. 10(a). To validate our control concept, we consider the following scenario, which implies a ramp-up strategy for the FFE process:

- (a) $t = 200$ s: Ramp up the Compressor power by stepping from its initial value $u_{2,0} = 0$ kW to $u_{2,d}$ calculated by (38b) with $\bar{z} = 0.35$ kg kg⁻¹ and $y_{1,d}, y_{2,d}$ according to Setpoint 1, see Section 4.2.
- (b) $t = 460$ s: Ramp up the input mass flow by stepping from its initial value $u_{1,0} = 2.7$ kg s⁻¹ to $u_{1,d}$ calculated by (38a) with $\bar{z} = 0.35$ kg kg⁻¹ and $y_{1,d}, y_{2,d}$ according to Setpoint 1, see Section 4.2.
- (c) $t = 1000$ s: Switch to u_1, u_2 calculated by the feedforward structure some time before the product enters the FFE at $t = 2000$ s.
- (d) $t = 2600$ s: Additionally, switch on the controllers C_1, C_2 when y_1, y_2 are close to their operation points.
- (e) $t = 4000$ s: Step from Setpoint 1 to Setpoint 2, see Section 4.2.
- (f) $t = 7000$ s: Step from Setpoint 2 to Setpoint 1, see Section 4.2.
- (g) $t = 9200$ s: Step of disturbance z due to feed tank exchange.

The corresponding results are depicted in Fig. 10 and Fig. 11, where Fig. 10 shows the ramp-up process and Fig. 11 the setpoint changes as well as disturbance response.

Firstly, note that the background colors in Fig. 10 and Fig. 11 have the following meanings:

- The red area corresponds to ramp-up of Compressor power and input mass flow, i.e., Items (a), (b).
- The blue area corresponds to control under pure feedforward structure, i.e., Item (c).

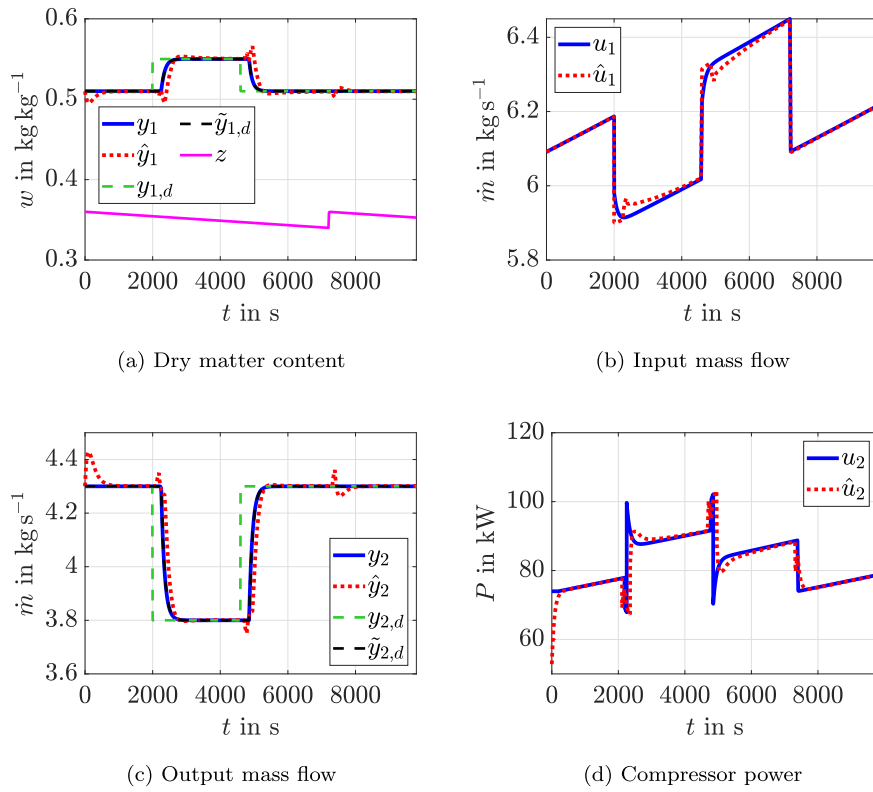


Fig. 9. Simulation results for exact parameters and nonexact ($\hat{\cdot}$)-parameters. (For interpretation of the references to color in this figure legend, the reader is referred to the web version of this article.)

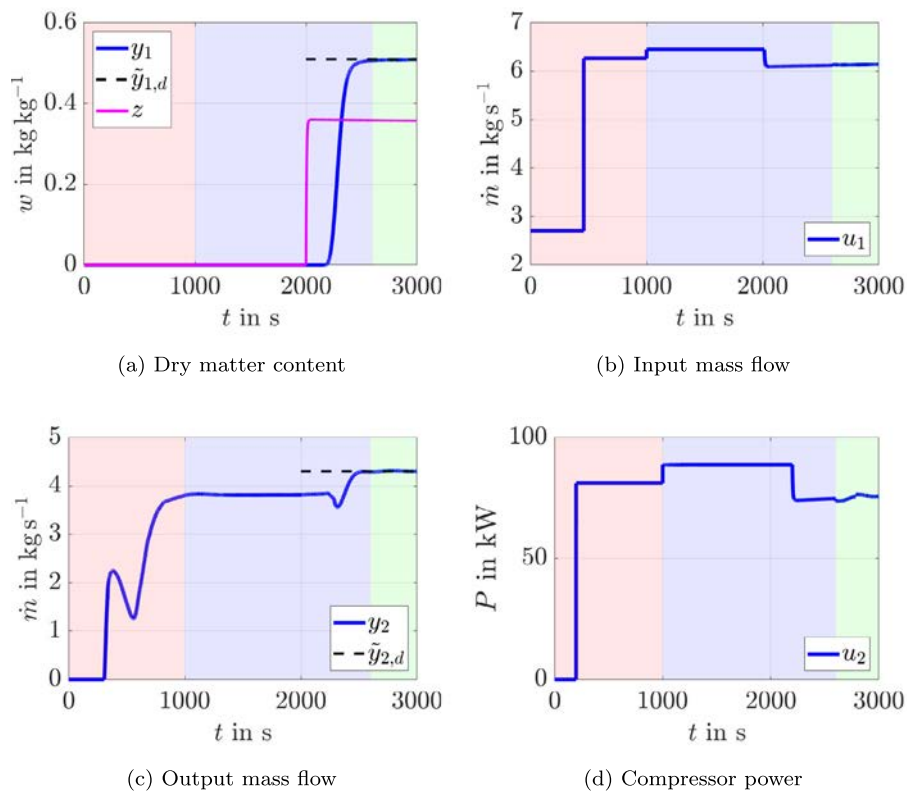


Fig. 10. Ramp-up of the FFE process via digital plant twin. (For interpretation of the references to color in this figure legend, the reader is referred to the web version of this article.)

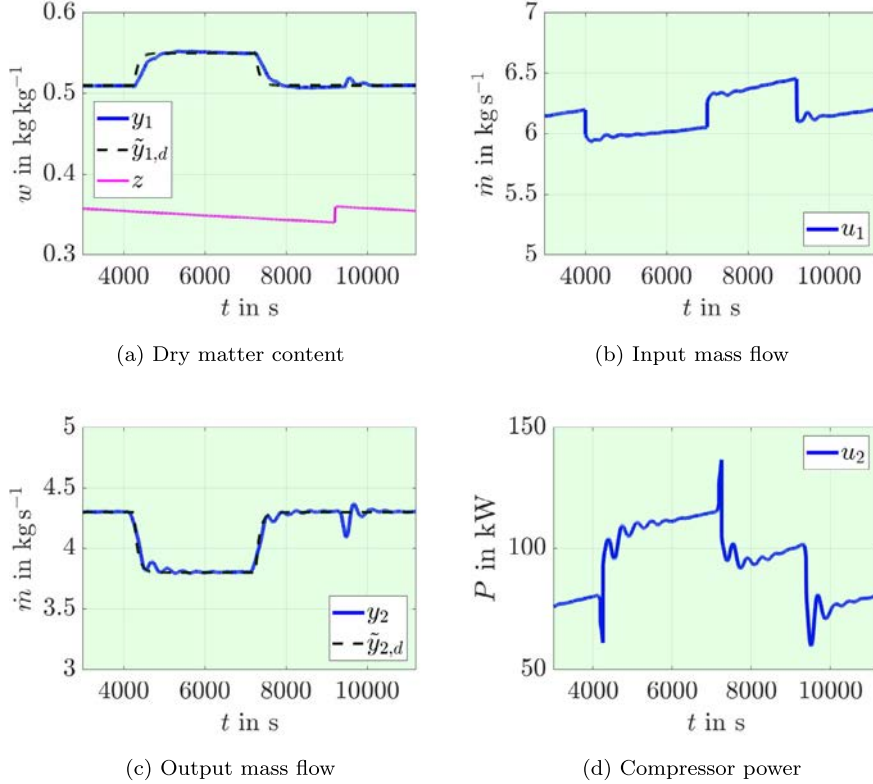


Fig. 11. Tracking and disturbance response of the FFE process via digital plant twin. (For interpretation of the references to color in this figure legend, the reader is referred to the web version of this article.)

- The green area corresponds to control under feedforward structure plus controllers, i.e., Items (d)–(g).

Secondly, note that the reference signals $\tilde{y}_{1,d}$, $\tilde{y}_{2,d}$ correspond to $y_{1,d}$, $y_{2,d}$ filtered by W_{11} , see (28).

In Fig. 10(a) and Fig. 10(c), it gets evident that the idea to ramp-up the process via pure feedforward structure yields a well-controlled transient behavior when product instead of water is introduced into the FFE at $t = 2000$ s. Furthermore, in Fig. 11(a) and Fig. 11(c), we observe that both tracking and disturbance response have satisfying behavior. Thus, we consider our concept to be validated.

6. Conclusions

In this paper, a new multivariable control concept for the falling film evaporator process is developed. As single-loop control of only w_o and manual ramp-up are common industrial practice, our concept additionally enables control of \dot{m}_o and an automated ramp-up process. Moreover, since our concept is represented in a block diagram structure, see Fig. 7, practical implementation into digital control systems is simplified. Consequently, it is readily accepted by plant operators and also cheaper for the customer than, e.g., model predictive controllers. In simulation studies, we show that our concept is robust to parametric and structural plant-model mismatches. Furthermore, via our digital twin of the plant, we conclude that our automated ramp-up strategy leads to smooth transient behavior during the critical process step when product instead of water enters the FFE. Therefore, future work on implementation to the real-world FFE process will be conducted.

CRedit authorship contribution statement

Julian Hofmann: Methodology, Software, Validation, Investigation, Data curation, Writing – original draft. **Anton Ponomarev:**

Methodology, Software, Formal analysis, Writing – review & editing. **Veit Hagenmeyer:** Funding acquisition, Project administration, Writing – review & editing. **Lutz Gröll:** Conceptualization, Supervision, Writing – review & editing.

Declaration of competing interest

The authors declare that they have no known competing financial interests or personal relationships that could have appeared to influence the work reported in this paper.

Acknowledgments

This work was supported by the Helmholtz Association under the program “Energy System Design”. Additionally, the authors thank GEA Wiegand GmbH for data and technical information regarding the falling film evaporator process.

Appendix A. Measurement of dry matter content

Throughout the paper, we implicitly assume that dry matter content w_i at the FFE's input and w_o at its output are both measured. However, more precisely, the liquid's dry matter content w is indirectly measured based on the measurements of the liquid's density ρ , temperature ϑ , and the static estimator

$$\hat{w}(\rho, \vartheta) = \left(\frac{1}{\hat{A}} \left(\frac{\rho}{\hat{A}_w + \hat{B}_w \vartheta + \hat{C}_w \vartheta^2} - 1 \right) \right)^{1/\hat{B}}, \quad (\text{A.1})$$

where $\hat{A}_w = 629.5$, $\hat{B}_w = 2.64$, $\hat{C}_w = -0.0047$, $\hat{A} = 0.369$, and $\hat{B} = 0.138$ are experimentally determined dimensionless fitting coefficients being valid for milk as liquid. Note that (A.1) is a quantity equation, i.e., all quantities are divided by their physical units. In case of (A.1), there is \hat{w} in kg kg^{-1} , ρ in kg m^{-3} , and ϑ

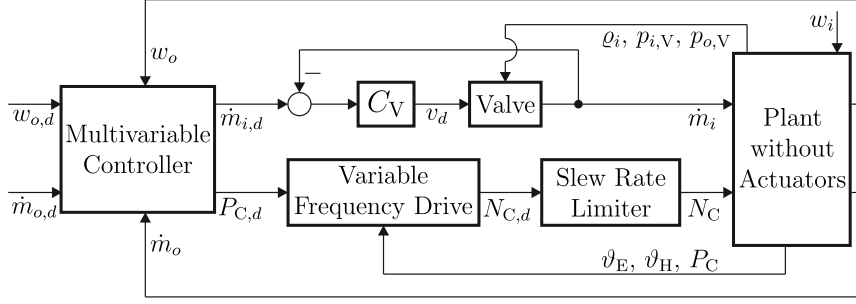


Fig. B.12. Closed-loop system with actuator dynamics.

in K. Hence, in our concept, we reject the disturbance $z = w_i$ and control the output $y_1 = w_o$ via indirect measurements of these quantities.

Appendix B. Actuator dynamics

Although actuator dynamics were neglected during the control design in Section 4, they are part of the real-world plant. Therefore, the actuator dynamics are modeled in this section and are included in the digital plant twin used for validation in Section 5.2. As observed in Section 4, the multivariable controller outputs the input mass flow $u_1 = \dot{m}_i$ and the power $u_2 = P_C$ supplied to the Compressor. In fact, since direct actuation of \dot{m}_i and P_C is not possible due to physical reasons, the multivariable controller outputs the corresponding desired values, i.e., $\dot{m}_{i,d}$ and $P_{C,d}$. For the sake of clearer representation, we disregard the control nomenclature introduced in Section 3.2 and instead consider all variables in physical nomenclature throughout this section.

In the first step, we clarify how $\dot{m}_{i,d}$ is adjusted via a control valve. Based on the deviation $\dot{m}_{i,d} - \dot{m}_i$, the PI controller

$$C_V(s) = k_{p,v} + \frac{k_{i,v}}{s} \quad (\text{B.1})$$

calculates the desired valve position $v_d \in [0, 1]$, which is the input to the Valve modeled by

$$\frac{d}{dt}v(t) = \frac{1}{T_V}(v_d(t) - v(t)), \quad (\text{B.2a})$$

$$K_v(t) = \begin{cases} 0, & v(t) \in [0, 0.02], \\ K_{v,s} n^{1-v(t)}, & v(t) \in [0.02, 1], \end{cases} \quad (\text{B.2b})$$

$$\dot{m}_i(t) = K_v(t) \sqrt{1000 \varrho_i(t) (p_{i,v}(t) - p_{o,v}(t))}, \quad (\text{B.2c})$$

cf. [42]. The pressures $p_{i,v}$, $p_{o,v}$, and input density ϱ_i are known via measurements. The constants $K_{v,s}$ and n determine the Valve's equal percentage characteristic curve whereas the time constant T_V is identified in preliminary experiments. Note that (B.2c) represents a quantity equation, i.e., all quantities in (B.2c) are divided by their physical unity, where \dot{m}_i in kg h^{-1} , K_v in kg h^{-1} , ϱ_i in kg m^{-3} , $p_{i,v}$ and $p_{o,v}$ in bar abs.

In the second step, we recall the Compressor model

$$P_C(t) = P_C(N_C(t), \vartheta_E(t), \vartheta_H(t)) \quad (\text{B.3})$$

given in [1] and explain how the desired power $P_{C,d}$ is converted into the rotational speed N_C . From the practical perspective, the programming of the Compressor's actuator, a variable frequency drive, needs to be adapted to manipulate P_C instead of N_C . As detailed modeling of the variable frequency drive is out of the paper's scope, we instead use the estimator

$$\begin{aligned} \frac{d}{dt}N_{C,d}(t) &= \frac{\dot{P}_{C,d}(t) - \frac{\partial P_C}{\partial \vartheta_E}(t) \dot{\vartheta}_E(t) - \frac{\partial P_C}{\partial \vartheta_H}(t) \dot{\vartheta}_H(t) - \alpha (P_C(t) - P_{C,d}(t))}{\frac{\partial P_C}{\partial N_{C,d}}(t)} \end{aligned} \quad (\text{B.4})$$

with $\alpha > 0$ to determine the Compressor's desired rotational speed $N_{C,d}$. Firstly, note that (B.4) is based on the method of dynamic inversion [43] applied to (B.3) with $N_C := N_{C,d}$, i.e., (B.4) is obtained from

$$\frac{d}{dt} \left(P_C(N_{C,d}(t), \vartheta_E(t), \vartheta_H(t)) - P_{C,d}(t) \right) = -\alpha (P_C(t) - P_{C,d}(t)). \quad (\text{B.5})$$

Secondly, note that in (B.4), derivatives $(\dot{\cdot})$ w.r.t. time t are implemented in combination with the corresponding filters to enable noise suppression. Downstream from the variable frequency drive, the slew rate limiter

$$\frac{d}{dt}N_C(t) = \begin{cases} r, & \text{if } \frac{d}{dt}N_{C,d}(t) > r \text{ or } N_{C,d}(t) > N_C(t), \\ -r, & \text{if } \frac{d}{dt}N_{C,d}(t) < -r \text{ or } N_{C,d}(t) < N_C(t), \\ \frac{d}{dt}N_{C,d}(t), & \text{otherwise} \end{cases} \quad (\text{B.6})$$

converts $N_{C,d}$ into the actual rotational speed N_C , where the constant r denotes the slew rate limit. Thus, the slew rate limiter (B.6) ensures that the steps required by the controller are converted into ramps. The closed-loop system with explicit distinction between plant and actuators is shown in Fig. B.12. In the upper loop of Fig. B.12, we observe a serial cascade control structure.

References

- [1] C. Schwaer, J. Hofmann, M. Mühlpfordt, A. Frank, L. Gröll, Modular simulation model for falling film evaporators with novel approach to manage dominant time-varying transport delays, *Comput. Chem. Eng.* 132 (2020) 106604.
- [2] J. Hofmann, A. Ponomarev, V. Hagenmeyer, L. Gröll, Transport models for liquid films, *Automatisierungstechnik* 68 (8) (2020) 625–640 (in German).
- [3] J. Hofmann, L. Gröll, V. Hagenmeyer, Control loop pairing and interaction analyses of the falling film evaporator process, in: 23rd International Conference on Process Control, IEEE, 2021, pp. 186–193.
- [4] J. Winchester, C. Marsh, Dynamics and control of falling film evaporators with mechanical vapour recompression, *Chem. Eng. Res. Des.* 77 (5) (1999) 357–371.
- [5] D. O'Callaghan, P. Cunningham, Modern process control techniques in the production of dried milk products – a review, *Le Lait* 85 (4–5) (2005) 335–342.
- [6] S. Paramalingam, Modelling, Optimisation and Control of a Falling-Film Evaporator (Ph.D. thesis), Massey University, New Zealand, 2004.

- [7] H.H. Bakker, C. Marsh, S. Paramalingam, H. Chen, Cascade controller design for concentration control in a falling-film evaporator, *Food Control* 17 (5) (2006) 325–330.
- [8] M. Karimi, A. Jahanmiri, Nonlinear modeling and cascade control design for multi effect falling film evaporators, *Iran. J. Chem. Eng.* 3 (2) (2006) 52–63.
- [9] M. Farsi, A. Jahanmiri, A new control algorithm for concentration control in three effect falling film evaporators, *Iran. J. Sci. Technol. Trans. B Eng.* 33 (B5) (2009) 387–396.
- [10] A. Haasbroek, W. Steyn, L. Auret, Advanced control with fundamental and data-based modeling for falling film evaporators, in: *International Conference on Industrial Technology*, IEEE, 2013, pp. 46–51.
- [11] M. Karimi, A. Jahanmiri, M. Azarmi, Inferential cascade control of multi-effect falling-film evaporator, *Food Control* 18 (9) (2007) 1036–1042.
- [12] X. Wang, C. Li, X. Chen, Disturbance rejection control for multiple-effect falling-film evaporator based on disturbance observer, *Trans. Inst. Meas. Control* 38 (6) (2016) 773–783.
- [13] Z. Stefanov, K. Hoo, Control of a multiple-effect falling-film evaporator plant, *Ind. Eng. Chem. Res.* 44 (9) (2005) 3146–3158.
- [14] N.T. Russell, *Dynamic Modelling of a Falling-Film Evaporator for Model Predictive Control* (Ph.D. thesis), Massey University, New Zealand, 1997.
- [15] S. Lahtinen, Identification of fuzzy controller for use with a falling-film evaporator, *Food Control* 12 (3) (2001) 175–180.
- [16] A. Haasbroek, L. Auret, W. Steyn, A comparison of control techniques for dairy falling film evaporators, *IFAC Proc. Vol.* 46 (32) (2013) 253–258.
- [17] Q. Meng, H. Zhang, M. Howarth, Performances comparison between real-time auto-tuning PID and conventional PID controller for a dairy industrial evaporation process control, in: *International Conference on Artificial Intelligence, Control and Automation Engineering*, DESTech Publications, Inc., 2019.
- [18] M. Van Wijck, P. Quaak, J. Van Haren, Multivariable supervisory control of a four-effect falling-film evaporator, *Food Control* 5 (2) (1994) 83–89.
- [19] P. Quaak, M. Van Wijck, J. Van Haren, Comparison of process identification and physical modelling for falling-film evaporators, *Food Control* 5 (2) (1994) 73–82.
- [20] N. Bekiaris-Liberis, M. Krstic, *Nonlinear Control under Nonconstant Delays*, SIAM, 2013.
- [21] D. Bresch-Pietri, J. Chauvin, N. Petit, Adaptive control scheme for uncertain time-delay systems, *Automatica* 48 (8) (2012) 1536–1552.
- [22] V. Léchappé, E. Moulay, F. Plestan, A. Glumineau, A. Chriette, New predictive scheme for the control of LTI systems with input delay and unknown disturbances, *Automatica* 52 (2015) 179–184.
- [23] N. Bekiaris-Liberis, M. Krstic, Stability of predictor-based feedback for nonlinear systems with distributed input delay, *Automatica* 70 (2016) 195–203.
- [24] A. Ponomarev, Nonlinear predictor feedback for input-affine systems with distributed input delays, *IEEE Trans. Automat. Control* 61 (9) (2015) 2591–2596.
- [25] O.J.M. Smith, A controller to overcome dead time, *ISA J.* 6 (1959) 28–33.
- [26] M.R. Matausek, A.D. Micic, A modified Smith predictor for controlling a process with an integrator and long dead-time, *IEEE Trans. Automat. Control* 41 (8) (1996) 1199–1203.
- [27] T. Liu, Y. Cai, D. Gu, W. Zhang, New modified Smith predictor scheme for integrating and unstable processes with time delay, *IEEE Proc. D* 152 (2) (2005) 238–246.
- [28] C. Grimholt, S. Skogestad, Should we forget the Smith Predictor? *IFAC-PapersOnLine* 51 (4) (2018) 769–774.
- [29] W. Michiels, S.-I. Niculescu, On the delay sensitivity of Smith predictors, *Internat. J. Systems Sci.* 34 (8–9) (2003) 543–551.
- [30] J. Barraud, Y. Creff, N. Petit, PI controllers performance for a process model with varying delay, in: *UKACC International Control Conference*, 2004.
- [31] G. Kreisselmeier, Two-degree-of-freedom control structure, *Automatisierungstechnik* 47 (6) (1999) 266–269 (in German).
- [32] J. Winchester, *Model Based Analysis of the Operation and Control of Falling-Film Evaporators* (Ph.D. thesis), Massey University, New Zealand, 2000.
- [33] C.-H. Clerget, N. Petit, Dynamic optimization of processes with time varying hydraulic delays, *J. Process Control* 83 (2019) 20–29.
- [34] C. Albert, H. Marschall, D. Bothe, Direct numerical simulation of interfacial mass transfer into falling films, *Int. J. Heat Mass Transfer* 69 (2014) 343–357.
- [35] P. Bandi, M. Modigell, S. Groß, A. Reusken, L. Zhang, Y. Heng, W. Marquardt, A. Mhamdi, On reduced modeling of mass transport in wavy falling films, *AIChE J.* 64 (6) (2018) 2265–2276.
- [36] A. Ponomarev, J. Hofmann, L. Gröll, Novel control-oriented models for liquid transport in falling film evaporator tubes, *Comput. Chem. Eng.* 152 (2021) 107376.
- [37] C.R. Kharangate, H. Lee, I. Mudawar, Computational modeling of turbulent evaporating falling films, *Int. J. Heat Mass Transfer* 81 (2015) 52–62.
- [38] A. Donaldson, A. Thimmaiah, Process modelling and optimization of design parameters in a falling film plate and frame evaporator, in: *COMSOL Conference*, 2016, pp. 1–9.
- [39] J. Hofmann, A. Ponomarev, V. Hagemeyer, L. Gröll, Time-delay identification and validation of a liquid film transport model based on pilot plant experiments, in: *11th International Symposium on Advanced Control of Chemical Processes*, IFAC, 2021 https://www.iai.kit.edu/downloads/2021-02-25_Hofmann-Julian_final.pdf.
- [40] M. Morari, Robust process control, *Chem. Eng. Res. Des.* 65 (6) (1987) 462–479.
- [41] D. Vrancic, D. Vrecko, D. Juricic, S. Strmcnik, Automatic tuning of the flexible Smith predictor controller, in: *American Control Conference*, Vol. 6, IEEE, 1999, pp. 3853–3857.
- [42] H. Auinger, J. Ehmman, L. Grütesen, J. Heinrich, M. Huk, K. Jürgens, W. Klein, A. Kuhn, B. Kujawski, D. Metz, A. Muschet, A. Nagel, H. Peters, R. Rölli, C. Schindler, K. Scholl, M. Schwind, J. Seckler, V. Seppendorf, F. Valentin-Rumpel, M. Voß, *VDI-Richtlinien: Strömungstechnische Kenngrößen von Stellgeräten und deren Bestimmung*, Tech. Rep. VDI 2173, Verein Deutscher Ingenieure, 2018, ICS 23.060.40.
- [43] N. Getz, J.E. Marsden, A dynamic inverse for nonlinear maps, in: *34th Conference on Decision and Control*, Vol. 4, IEEE, 1995, pp. 4218–4223.

Repository KITopen

Dies ist ein Postprint/begutachtetes Manuskript.

Empfohlene Zitierung:

Hofmann, J.; Ponomarev, A.; Hagenmeyer, V.; Gröll, L.
[A new multivariable control concept for the falling film evaporator process.](#)
2021. Journal of process control, 106.
doi: [10.5445/IR/1000137336](#)

Zitierung der Originalveröffentlichung:

Hofmann, J.; Ponomarev, A.; Hagenmeyer, V.; Gröll, L.
[A new multivariable control concept for the falling film evaporator process.](#)
2021. Journal of process control, 106, 72–83.
doi: [10.1016/j.jprocont.2021.08.015](#)

Lizenzinformationen: [CC-BY-NC ND 4.0](#)